Maksym Dosta
Sergiy Antonyuk
Stefan Heinrich

Hamburg University of Technology, Institute of Solids Process Engineering and Particle Technology, Hamburg, Germany.

Research Article

Multiscale Simulation of the Fluidized Bed Granulation Process

A novel multiscale modeling approach was developed, implemented as basis of a simulation environment and applied to the fluidized bed spray granulation process. The high detailing level of the simulation is based on the process description on different time and length scales which are coupled by interscale communication laws. This allows considering a higher amount of process parameters, compared to the semi-empirical models which are typically used. The developed concept represents the production plant as flow sheet, with its further dynamic simulation on the macroscale. The influence of parameters such as viscosity of the sprayed suspension, nozzle positions, and temperature of the fluidization air on the whole process can be considered on the microscale.

Keywords: Discrete element modeling, Flowsheet simulation, Fluidized bed spray granulation, Multiscale simulation

Received: February 08, 2012; *accepted:* March 19, 2012

DOI: 10.1002/ceat.201200075

1 Introduction

Fluidized bed (FB) spray granulation is one of the most important production processes in the solids industry. Despite the wide usage of this process and the huge experimental and analytical work which has been performed in recent decades, considerable gaps still exist in the process understanding. Due to the rapid development of modern computer systems, nowadays the numerical simulation is a basic tool to analyze and predict the behavior of production plants. The simulation parallel with an analysis of experimental data allows better process understanding in order to analyze the influence of different parameters and to develop control strategies. This provides a possibility to avoid or to minimize the amount of expensive experiments.

The main problem of numerical modeling of industrial solids processes is a gap between the scales, where detailed models, based on the material microproperties, exist and the production scale as the point of interest for practical application [1]. Most industrial studies are based on process modeling with usage of empirical or semi-empirical models, enabling to obtain a solution in acceptable time. However, empirical models have a limited accuracy level and relatively small parameter space, where such models can be effectively used.

To increase the accuracy of process description and to allow considering the material microproperties and geometric specifications of apparatuses, the submodels which are relevant at different time and length scales can be combined by interscale communication algorithms into one multiscale model. In recent years, different authors have applied multiscale modeling to different solids processes and solids processing apparatuses such as drum granulators [2], crystallizers [3], fluidized-bed reactors [4], and gas-solid fluidization [5]. However, neither of the existing systems can be effectively applied for the fluidized-bed granulation process or extended to other solids processes.

The fast growth of the number of scientific contributions in the area of multiscale simulation of solids emphasizes the growing interest for such approach. The crucial factor of this progress is the continuous increase of computer performances and the wide distribution of parallel computing (multicore systems, GPU computing, specialized high-performance centers). In the authors' opinion, in the next few years the above described factors will cause an appearance of the various multiscale simulation systems for solids processes.

2 Multiscale Process Treatment

A typical production plant contains different apparatuses and machineries connected by mass and energy streams. Nowadays, the usage of flowsheet simulation systems for numerical solution of the energy and the mass balances in such plants is state-of-the-art. Especially for dynamic simulations of solids processes the system SolidSim-Dynamics has been developed [6]. In the current work, the modeling of an FB granulator, based on the detailed multiscale simulation environment, was performed. The new model of the FB apparatus consists of three submodels at different scales of the process description (Fig. 1). The arrows in the scheme represent the interscale communications and the list of the transferable parameters.

Correspondence: M. Dosta (dosta@tuhh.de), Hamburg University of Technology, Institute of Solids Processes Engineering and Particle Technology, Denickestraße 15, 21073 Hamburg, Germany.

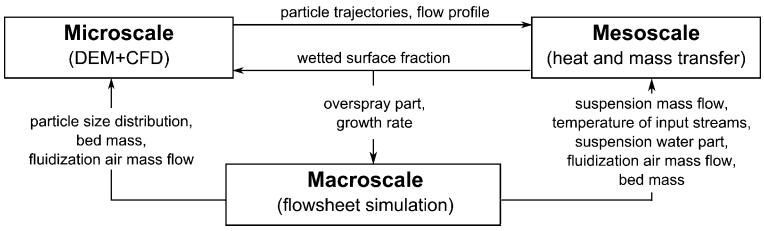

Figure 1. Interscale coupling.

The macroscale model is based on the 1D population balance model (PBM), where the change of the particle size distribution (PSD) is described by partial differential equations. The application of one of the various numerical approximation schemes, such as the method of moments, method of characteristics, finite difference scheme, etc., allows attaining the solution of the PBM in a relatively short period of time. The parameters of PBM, such as the size-independent growth rate, are commonly obtained empirically and do not consider the specific apparatus or the material properties which can decrease the model correctness. With the purpose to obtain more predicted modeling results, models on the micro- and mesoscales have been used.

Macroscale modeling was implemented in the flowsheet simulation system SolidSim-Dynamics. The calculations in this system are performed with a sequential-modular approach, which allows the usage of closed-form mathematical models for the description of different apparatuses or process substeps [7]. Therefore, simultaneously to the application of a detailed multiscale model for the description of granulation, the semi-empirical models for the apparatuses of the periphery, such as screens, mill, etc., have been used.

On the microscale, the particle movement and their interactions in the fluid flow are simulated. The particle motion is calculated by the discrete element method (DEM), where each granule is considered as separate entity and in every time step the Newtonian equations of motion are solved. The simulation of the gas phase is based on the Navier-Stokes equations and is performed using the computational fluid dynamics (CFD) system. The simultaneous cosimulation of the gas and solid phases is realized through the coupling of DEM and CFD systems. On the one hand, the drag force and pressure gradient, which are acting on the particle, are obtained in the CFD system and used in the DEM calculations, on the other hand, the recalculated cell porosities due to the existence of particles are used in the CFD system.

The mesoscale model serves as an intermediate submodel between micro- and macroscales. One part of it is used to calculate the particle wetting with the help of a model, based on the description of the spraying zone in the granulator [8]. In terms of mass and energy balances, the second part of the mesoscale model describes the heat and mass transfer between the air, liquid film, and particles. Fig. 2 presents the algorithm which was implemented into the newly developed MUltiscale Simulation ENvironment called "MUSEN". To avoid the inequality between values on the different scales, the global calculation time is divided into a set of time intervals (windows) with a size WT_{macro}. Afterwards, the simulation is starting on the macroscale (block 2) and is performed for the specific time interval (CT; CT+WT_{macro}). According to the received values on the macroscale, the microscale model is generated.

Due to the high computational effort of DEM and CFD systems, the microscale calculation (block 4) is performed for a short time interval in the order of seconds (WT_{micro}). As a result, the particle trajectories and the time-dependent fluid profiles are obtained in the apparatus and are transmitted into the mesoscale. Here, it is assumed that the particles cyclically repeat their trajectories on the longer time interval (WT_{meso}) which allows to run further mesoscale calculations (block 5) for a longer time interval without usage of the time-consuming DEM and CFD methods.

On the mesoscale, the wetting and the drying processes are modeled. The obtained wetted surface fraction φ describes the part of the particle surface which is covered by a liquid film. The existence of the liquid leads to viscous and capillary forces acting in the particle contacts and can have a significant effect on the particle dynamics [9]. Therefore, these forces must be considered on the microscale in the DEM simulation.

After calculations in the blocks 4 and 5, the significant difference can appear between values of φ on the micro- and mesoscales. That is why the further reiteration is necessary and it is repeated until the convergence is reached (block 3). Finally, the size-dependent growth rate is obtained and used in the PBM to repeat the calculations of the granulation process on

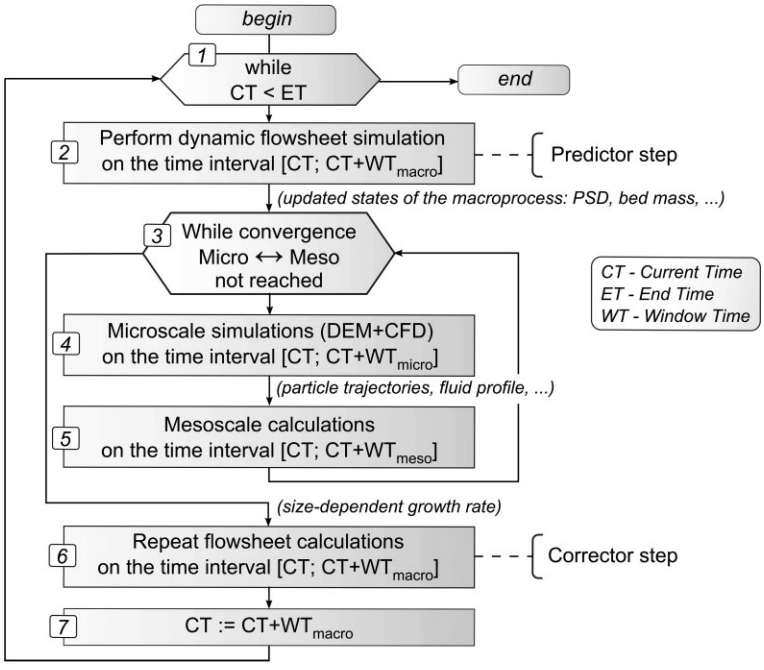

Figure 2. Flow chart of the main calculation algorithm.

the current time interval (block 6). The algorithm presented in Fig. 2 allows the use of different internal calculation time steps for the numerical solution of different models. The difference between magnitudes of the steps can reach several orders which can essentially decrease the amount of computations. Therefore, there is no necessity to perform simulations of the whole plant in a time interval, which is in the order of hours, with an internal step of the DEM being typically in the range of few microseconds.

3 Submodels on the Different Scales

3.1 Microscale

In each simulation time step of the DEM, the new coordinates of the particles and their rotational motion are predicted by calculation of the Newtonian equations of motion. In Eq. (1), the general form of the translation motion equation is given by:

$$m\frac{\mathrm{d}^2 r}{\mathrm{d}t^2} = F_\mathrm{D} + F_\mathrm{G} + \sum_{\mathrm{i}=1}^{\mathrm{N_{cp}}} F_{\mathrm{cp,i}} + \sum_{\mathrm{i}=1}^{\mathrm{N_{cw}}} F_{\mathrm{cw,i}} \quad (1)$$

where F_D and F_G are the drag and gravity forces, respectively; $F_{\mathrm{cp,i}}$ and $F_{\mathrm{cw,i}}$ are forces due to contacts with other particles and apparatus walls; N_{cp} and N_{cw} are the number of contacts.

For calculation of the forces in a dry contact, the Hertz-Mindlin model is used. The normal component of the force described by the Hertz model was supplemented with a damping term according to Tsuji et al. [10]. The tangential force was calculated by a model proposed by Mindlin and Deresiewicz [11]. These models were originally developed for interactions between dry particles and cannot predict the impact behavior when a liquid film on the particle surface exists. The significant influence of the liquid bridges on the collisional behavior of the particles is described in several publications [9, 12–16].

One possible way to consider the liquid phase in the model of the spray granulation process is the increase of the energy dissipation during collisions. This can be realized by decreasing of the restitution coefficient with further parameter fitting to the experimental data [9, 17]. However, only a fitting of the restitution coefficient without the improvement of the contact models cannot correctly predict the real contact forces and the particle dynamics during injection of the liquid in the granulator. The main difference between dry and wet contacts is caused by the fact that the capillary and viscous forces act on the particles before and after the contact of solid phases. Therefore, in the performed DEM simulation, the Hertz-Mindlin contact model was extended by viscous F_{vis} and capillary F_{cap} forces. The interaction distance, where the contact detection and the force calculation take place, was increased according to the assumed liquid film thickness and the liquid bridge rupture distance. Fig. 3 indicates the induced forces in some collision modes.

The normal and the tangential components of the viscous force were calculated using Eqs. (2) and (3), respectively [18, 19].

$$F_{\mathrm{vis}}^{\mathrm{n}} = \frac{6\pi\eta\bar{R}^2 v_{\mathrm{n,rel}}}{L} \quad (2)$$

$$F_{\mathrm{vis}}^{\mathrm{t}} = 2\pi\eta\bar{R}v_{\mathrm{t,rel}}\ln\left(1+\frac{\bar{R}}{2L}\right) \quad (3)$$

$$\bar{R} = R_1R_2/(R_1+R_2) \quad (4)$$

where R_1 and R_2 are the radii of the contact partners; $v_{\mathrm{n,rel}}$ and $v_{\mathrm{t,rel}}$ describe the normal and tangential components of the relative impact velocity; η is the liquid viscosity. The distance between particle surfaces L was limited by the minimum value of $L = 2h_\mathrm{a}$, where h_a is the particle roughness.

The capillary force depends on the surface tension σ, the volume of the liquid bridge V, and the solid/liquid contact angle θ, and is calculated by Eq. (5) according to the model of Pitois et al. [12]. The experimental observations of the capillary forces in the liquid bridges were also reported by Butt and Kappl [20].

$$F_{\mathrm{cap}} = 2\pi\bar{R}\sigma\cos\theta\left(1-\left(1+\frac{2\cdot V}{\pi\cdot\bar{R}\cdot L^2}\right)^{-0.5}\right) \quad (5)$$

During an FB granulation process with liquid injection, the particle surface is just partially covered by a liquid film. Therefore, dry and wet collisions simultaneously take place in the FB. To describe the different collision types, according to the value of the wetted surface fraction (φ), the probabilities of different events were calculated. Each new collision was randomly arranged to the specific type of collision, as it is indicated in Fig. 4.

The collision is considered to be finished when the rupture of the liquid bridge occurs. It takes place when a critical bridge length is reached. It was assumed that the critical length equals a distance of the double initial thickness of the liquid film in the contact. Each further contact between the same particles arranged anew, according to the scheme in Fig. 4.

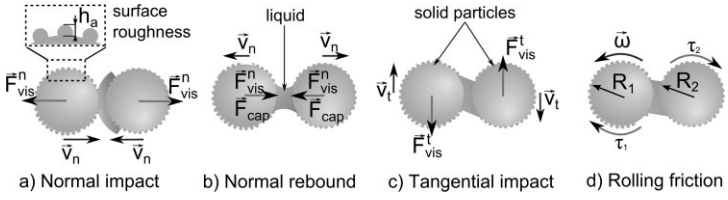

Figure 3. Different types of impact of wetted particles.

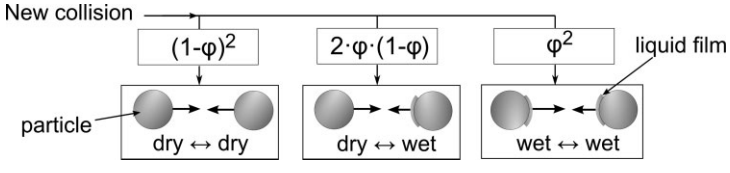

Figure 4. Probabilities of different collision types.

3.2 Mesoscale

In comparison with the microscale model, the mesoscale calculations have been performed at the same length but at a larger time scale. Here, the particles were considered as separate entities and the heat and mass transfer between all three phases were calculated. As the input data for the mesoscale model, the basic plant parameters such as the suspension mass flow, temperature of all streams etc., and the particle trajectories and flow velocities have been received from the microscale. Assuming that the particles repeat their trajectories, the calculations of the wetting and drying have been performed for a long time period.

To describe the wetting of a particle with a suspension, the simplified nozzle model is implemented. The wetting region is represented as a cone zone and is discretized through the height into a set of layers. In each simulation time step, the porosities in all layers are recalculated. The amount of the liquid, which reaches the particle surface, depends on the particle cross-cut area, relative position of the particle in the wetting zone, and porosity of the upper layers. The droplets which do not impact with particles or do not collide with an apparatus wall are considered in the energy and mass balance and, after drying, the solid part of them leaves the apparatus as overspray dust.

Based on the energy and mass balances, the differential equations for the description of particle temperature ϑ_p, liquid film temperature ϑ_f, mass of the liquid film M_f, air temperature ϑ_a, and air humidity Y_a were formulated. Eqs. (6)–(8) were solved for each particle. Here, the following heat ($\dot{Q}$) and enthalpy streams ($\dot{H}$) are considered: (i) between air and particle $\dot{Q}_{ap}$; (ii) between air and liquid film $\dot{Q}_{af}$; (iii) between a particle and liquid film $\dot{Q}_{pf}$; and (iv) enthalpy streams of a vapor ($\dot{H}_{vap}$) and a suspension ($\dot{H}_{susp}$).

The heat and mass transfer coefficients were calculated according to the model of Gnielinski [21].

$$\frac{d\vartheta_p}{dt} = \frac{\dot{Q}_{ap} - \dot{Q}_{pw}}{M_p c_{p,p}} \tag{6}$$

$$\frac{d\vartheta_f}{dt} = \frac{\dot{Q}_{pf} + \dot{Q}_{af} + \dot{H}_{susp} - \dot{H}_{vap}}{M_f c_{p,f}} - \frac{\vartheta_{film}}{M_f}\frac{dM_f}{dt} \tag{7}$$

$$\frac{dM_f}{dt} = \dot{M}_{susp} - \dot{M}_{vap} \tag{8}$$

To describe the gas phase on the mesoscale, the apparatus was discretized above the height into a set of layers, and for each layer, differential equations for the description of the air temperature and air humidity were solved.

As a result from the mesoscale simulation, the averaged wetted surface fraction ϕ and the specific growth rate $G_{e,i}^{meso}$ for each particle were obtained by Eqs. (9) and (10).

$$\phi = \sum_{i=1}^{N_p} \frac{M_{f,i}}{\rho_f L_f A_{p,i} N_p} \tag{9}$$

$$G_{e,i}^{meso} = \frac{(1 - K_w)\dot{M}_{vap,i}}{2\rho\pi R_{p,i}^2 K_w} \tag{10}$$

where L_f is the thickness of the liquid film; N_p is the total number of particles; $A_{p,i}$ is the surface of a specific particle; K_w is the water mass content in suspension, and $R_{p,i}$ is the particle radius.

3.3 Macroscale

Here, granulation was described as a pure growth process with attrition, without taking into account aggregation and breakage terms. As the mathematical model of FB granulation, a 1D population balance model (PBM) with particle diameter as the internal property coordinate was used. The main equation for description of time progression of particle size distribution (PSD) during the granulation process has the following form:

$$\frac{\partial n(t,d)}{\partial t} = -\frac{\partial\left[\left(G_e^{macro}(t,d) - \mathrm{Attr}(t,d)\right)n(t,d)\right]}{\partial d} + \dot{n}_{in}(t,d) - \dot{n}_{out}(t,d) \tag{11}$$

where $\frac{\partial n(t,d)}{\partial t}$ is the change of the particle number over time; the term $G_e^{macro}(t,d)$ describes the particle growth; $\mathrm{Attr}(t, d)$ is used to consider the attrition of granules; $\dot{n}_{in}(t,d)$ and $\dot{n}_{out}(t,d)$ characterize the particle fluxes entering and leaving the apparatus, respectively.

The growth rate on the macroscale G_e^{macro} is one of the main parameters which determines the behavior of the PBM. In a previous work [22], the simplified semi-empirical model was used which assumes that all particles have the same growth rate regardless of the size, expressed as:

$$G_e^{macro} = \frac{2\dot{M}_e}{\rho_p A_{tot}} = \frac{2\dot{M}_{susp}(1 - K_{os})(1 - K_w)}{\rho_p A_{tot}} \tag{12}$$

where $\dot{M}_e$ is the effective mass flow of suspension, ρ_p is the particle density, A_{tot} is the total surface of all particles in the granulator, K_w is the water content in the suspension, and K_{os} is the mass part of the overspray.

However, the assumption of the size-independent growth would drastically decrease the accuracy of the developed mathematical model. Due to the different factors, as, e.g., unequal residence time in the spraying zone for different particles classes, the granules have different growth rates, as experimentally observed by Zank [23]. Therefore, in the developed simulation system, the parameters G_e^{macro} and K_{os} were directly obtained from the simulation on the lower scales.

For the calculation of other apparatuses involved in the production process, semi-empirical models have been used. Both screens (see Fig. 5) have been simulated based on the Plitt separation model [24]. The grade efficiency in this model is calculated as a function of cut size (d_{cut}) and separation sharpness (a) and expressed as:

$$T(d) = 1 - \exp\left(-0.693\left(\frac{d}{d_{cut}}\right)^a\right) \tag{13}$$

A size reduction short-cut model was used for the description of particle milling [6].

4 Production Process Simulation

In Fig. 5, the general flowsheet of the process is presented, which has been simulated with the multiscale simulation approach. This continuous process consists of an interconnection of four different apparatuses. The suspension is sprayed into the FB apparatus, where due to its drying on the granule surface the subsequent growth occurs. About 40 % of the output mass flow from the granulator reaches the stack of two screens, where the sieving of particles occurs. The oversize fraction of the first screen is milled and mixed with the undersize fraction of the second screen, and the combined stream is recycled into the apparatus. It is assumed that the mass of the holdup in the apparatus remains constant during the whole process. In Tab. 1, the simulation parameters used for calculation of the granulation process are listed.

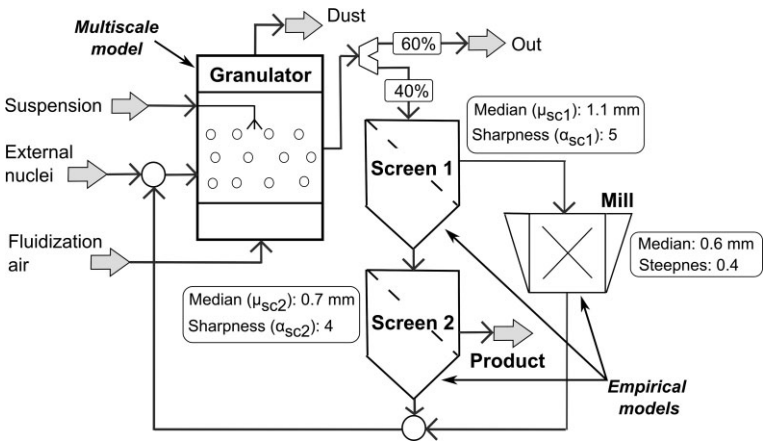

Figure 5. Flow sheet of the simulated production process.

Table 1. Main simulation parameters of the flowsheet in Fig. 5.

FB granulator	
Initial bed mass	0.245 kg
Initial PSD median	1 mm
Initial PSD standard deviation	0.1 mm
Fluidization air	
Temperature	80 °C
Suspension	
Mass flow	0.5 kg h^{-1}
Temperature	60 °C
Water content	50 %
External feed stream of nuclei	
Mass flow	1 kg h^{-1}
Temperature	30 °C
PSD median	0.6 mm
PSD standard deviation	0.1 mm

Instead of the fully dynamic simulation with splitting of a whole time interval into windows (see Fig. 2), the aim of the presented case study was to obtain more precise estimation of the steady-state regime of the process. That is why in the first iteration of the main algorithm in Fig. 2 the process was calculated on the macroscale in the flow sheet simulation system SolidSim-Dynamics up to steady-state. Here, the 1D PBM with the size-independent growth rate was used. To solve the partial differential equation, Eq. (11) was discretized and afterwards the system of ODE's was solved by variable-order, variable-coefficient backward differentiation formula, in fixed-leading-coefficient form [25].

In Fig. 6a, the time progression of the PSD in the apparatus is illustrated. In Fig. 6b, the output mass stream from the granulator and the product mass stream obtained from the simulation are plotted. After ~3 h, the process reaches the steady state, and the calculations on the lower scales starts.

The steady-state results (PSD and input mass flows) obtained from the SolidSim-Dynamics were used as initial conditions for the coupled DEM-CFD calculations. In Fig. 7, the front and top view of the apparatus used for the iterative calculations on the micro- and mesoscales are displayed. The top-spray configuration with three symmetrical nozzles was applied.

On the microscale, the DEM-CFD simulation with 25 000 particles was performed for the time interval of 9 s, where for the DEM calculations the fixed time step of 1 µs was used. The received results were taken to calculate the wetting and drying on the mesoscale for a longer time interval of 300 s under the assumption that the particles repeat their trajectories. For the numerical solution of the mesoscale model, the Euler method with variable time step size in the range between (1 ms; 0.1 s) was used. Afterwards, according to the main calculation algorithm (Fig. 2), the interscale iterations were repeated until the

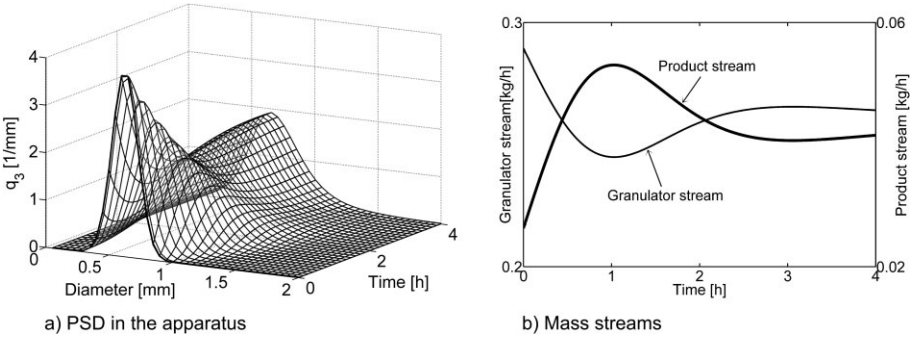

Figure 6. Simulation results on the macroscale.

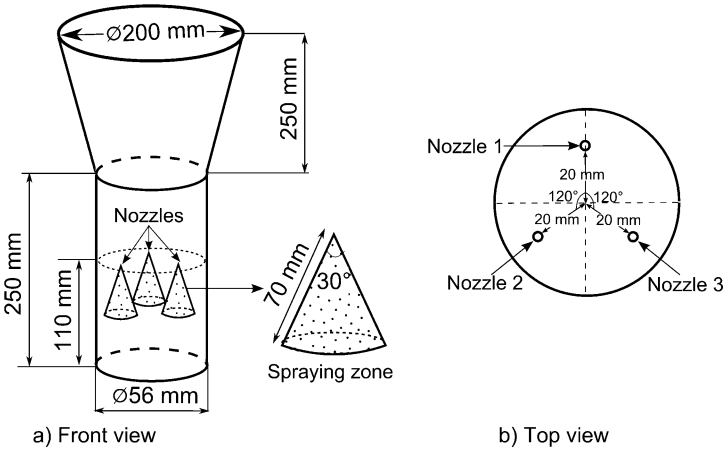

Figure 7. Apparatus geometry used for the micro- and mesoscale simulations.

convergence was reached. The screenshot in Fig. 8 illustrates the particle wetting in the FB apparatus. The particles are colored according to the deposited mass of the liquid film. It is assumed that the liquid film has a constant thickness of 0.1 mm.

The normalized growth rate $G_{\mathrm{norm}}^{\mathrm{meso}}(d)$ is plotted in Fig. 9. It was obtained according to Eq. (14), where $G_{\mathrm{norm}}^{\mathrm{meso}}(d)$ is calculated by Eq. (10). This parameter is used in the PBM to qualitatively estimate the difference between growth rates of granules with different sizes.

By solving of the implicit algebraic equation system in Eq. (15), the macroscopic growth rates $G_{\mathrm{e,i}}^{\mathrm{macro}}$ for different classes of PSD are calculated.

$$G_{\mathrm{norm}}^{\mathrm{meso}}(d) = \frac{G_{\mathrm{e}}^{\mathrm{meso}}(d)}{d_{\max} - d_{\min}} \int_{d_{\min}}^{d_{\max}} G_{\mathrm{e}}^{\mathrm{meso}}(d)\,dd \tag{14}$$

$$\begin{cases} G_{\mathrm{norm}}^{\mathrm{macro}}(d) = G_{\mathrm{norm}}^{\mathrm{meso}}(d) \\ \sum G_{\mathrm{e,i}}^{\mathrm{macro}}(d)\, A_{\mathrm{i}}(d) = \dfrac{2\dot{M}_{\mathrm{susp}}(1-K_{\mathrm{os}})(1-K_{\mathrm{w}})}{\rho_{\mathrm{p}}} \\ G_{\mathrm{norm}}^{\mathrm{macro}}(d) = \dfrac{G_{\mathrm{e}}^{\mathrm{macro}}(d)}{d_{\max} - d_{\min}} \int_{d_{\min}}^{d_{\max}} G_{\mathrm{e}}^{\mathrm{macro}}(d)\,dd \end{cases} \tag{15}$$

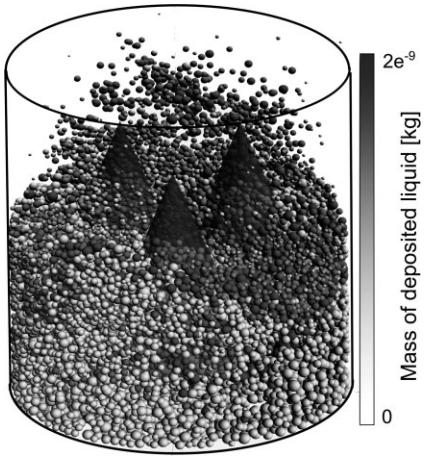

Figure 8. Simulation results of particle wetting in the FB apparatus.

The overspray part of the suspension (K_{os} = 0.063) was directly obtained from the mesoscale calculations, as expressed in Eq. (16):

$$K_{\mathrm{os}} = \frac{\dot{M}_{\mathrm{os}}}{\dot{M}_{\mathrm{susp}}} \tag{16}$$

From the received results, the conclusion can be drawn that in the investigated process the smaller particles have a higher growth rate. This occurs due to the top-down configuration of suspension injection and the partial segregation of the bed material. The larger particles have a longer residence time in the bottom zones of the apparatus and, as a consequence, a smaller amount of the suspension drops collides with these granules.

In the last step of the main simulation algorithm (Fig. 2), the flowsheet calculations were performed with predicted values of a growth rate and an overspray part of the suspension. In Fig. 10, the PSDs obtained with the empirical model and detailed multiscale model are compared.

From the analysis of the obtained simulation results it can be concluded that consideration of the size-dependent growth,

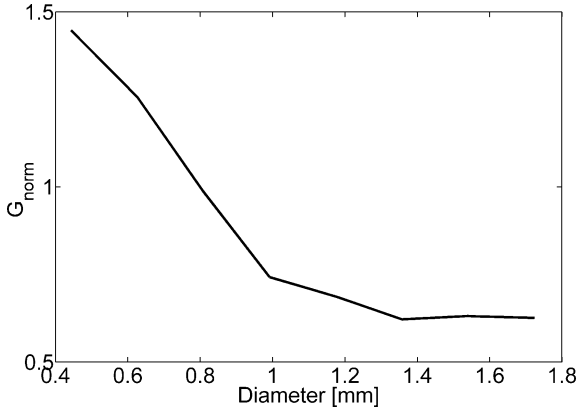

Figure 9. Size-dependent growth rate.

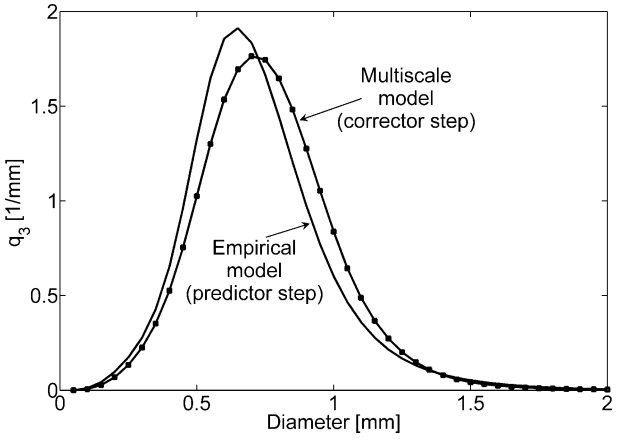

Figure 10. Comparison between steady-state results of empirical and multiscale models.

where smaller particles grow faster, results in a coarser PSD in the FB. This happens due to the fast enlargement of the fine fractions, which are supplied into the apparatus as a recycled stream, and due to the slow enlargement of coarse particles. This causes a smaller mass stream of the solid, which is milled as an oversize of the first screen and, as a consequence, a smaller amount of fine particles which are recycled into the granulator.

5 Conclusions

A novel simulation concept for calculation of the FB granulation process is presented and implemented into the multiscale simulation environment. This approach, where the interscale coupling plays a key role, allows reaching the ultimate goal of process modeling, namely the calculation of the whole production plant. In distinction to the existing simulation system, where mostly just empirical or semi-empirical models are used, the new concept allows considering the material microproperties and specific apparatus geometries.

The implemented multiscale model of the granulation consists of three submodels on different time or length scales. During process simulation, the iterative calculations of these models for different time intervals are performed. Finally, the population balance model with physically based parameters is applied in a flowsheet simulation system to predict the behavior of the whole plant on the macroscale. Similarly to the FB granulation process, the developed system can be extended and effectively applied for other apparatuses and other types of production processes in the solids industry.

The authors have declared no conflict of interest.

Symbols used

A	[m^2]	surface
Attr	[$m\,s^{-1}$]	attrition rate
c_p	[$J\,kg^{-1}K^{-1}$]	heat capacity
F	[N]	force
G	[$m\,s^{-1}$]	growth rate
$\dot{H}$	[$J\,s^{-1}$]	enthalpy stream
h_a	[m]	roughness
L	[m]	length
M	[kg]	mass
R	[m]	radius
v	[$m\,s^{-1}$]	velocity

Greek letters

ϑ	[°C]	temperature
η	[Pa s]	viscosity
σ	[$N\,m^{-1}$]	surface tension
φ	[–]	wetted surface fraction

Superscripts

n	normal
t	tangential

Subscripts

a	air
cap	capillary
D	drag
e	effective
f	liquid film
G	gravity
ml	mill
os	overspray
p	particle
sc1	screen 1
sc2	screen 2
susp	suspension
vap	vapor
vis	viscous

Abbreviations

DEM	discrete element method
FB	fluidized bed
PBM	population balance model
PSD	particle size distribution

References

[1] J. Werther, S. Heinrich, M. Dosta, E.-U. Hartge, *Particuology* **2011**, *9*, 320.
[2] G. D. Ingram, I. T. Cameron, *Proc. of ESCAPE – 15 Conf.* (Eds: L. Puigjaner, A. Espuna), Elsevier, Amsterdam **2005**.
[3] V. Kulikov, H. Briesen, W. Marquardt, *Chem. Eng. Res. Des.* **2005**, *83*, 706.
[4] S. Balaji, J. Du, C. M. White, B. E. Ydstie, *Powder Technol.* **2010**, *199*, 23.
[5] W. Ge, W. Wang, N. Yang, J. Li et al., *Chem. Eng. Sci.* **2011**, *66*, 4426.
[6] M. Dosta, S. Heinrich, J. Werther, *Powder Technol.* **2010**, *204*, 71.
[7] W. Marquardt, *Proc. of Chemical Process Control CPC-IV* (Eds: Y. Arkun), AIChE, New York **1991**.
[8] L. Fries, M. Dosta, S. Antonyuk, S. Heinrich, S. Palzer, *Chem. Eng. Technol.* **2011**, *34*, 1076.
[9] S. Antonyuk, S. Heinrich, N. Deen, H. Kuipers, *Particuology* **2009**, *7*, 245.
[10] Y. Tsuji, T. Tanaka, T. Ishida, *Powder Technol.* **1992**, *71*, 239.
[11] R. D. Mindlin, H. Deresiewicz, *J. Appl. Mech.* **1953**, 20.
[12] B. J. Ennis, G. Tardos, R. Pfeffer, *Powder Technol.* **1991**, *65*, 257.
[13] O. Pitois, P. Moucheront, X. Chateau, *J. Colloid Interface Sci.* **2000**, *231*, 26.
[14] S. J. R. Simons, X. Pepin, D. Rossetti, *Int. J. Miner. Process.* **2003**, *72*, 463.
[15] A. A. Kantak, R. H. Davis, *Chem. Eng. Sci.* **2006**, *61*, 417.
[16] C. D. Willett, A. J. Simon, M. J. Adams, J. P. K. Seville, in *Handbook of Powder Technology* (Eds: A. D. Salman, M. Ghadiri, M. J. Hounslow), Elsevier, Amsterdam **2007**.
[17] M. S. van Buijtenen, N. G. Deen, S. Heinrich, S. Antonyuk, J. A. M. Kuipers, *Can. J. Chem. Eng.* **2009**, *87*, 308.

[18] M. J. Adams, B. Edmondson, in *Tribology in Particulate Technology* (Eds: B. J. Briscoe, M. J. Adams), Adam Hilger, Bristol **1987**.
[19] V. L. Popov, *Contact Mechanics and Friction: Physical Principles and Applications*, 1st ed., Springer, Berlin **2010**.
[20] H.-J. Butt, M. Kappl, *Adv. Colloid Interface Sci.* **2009**, *146*, 48.
[21] V. Gnielinski, *Chem. Ing. Tech.* **1980**, *52*, 228.
[22] S. Heinrich, L. Mörl, *Chem. Eng. Process.* **1999**, *38*, 635.
[23] J. Zank, *Ph. D. Thesis,* Universität Karlsruhe **2003**.
[24] L. R. Plitt, *CIM Bull.* **1976**, *69*, 114.
[25] K. E. Brenan, S. L. Campbell, L. R. Petzold, *Numerical Solution of Initial-Value Problems in Differential-Algebraic Equations*, 2nd ed., SIAM, New York **1996**.

